SCIENTIFIC REPORTS
nature research

OPEN

Early animal evolution and highly oxygenated seafloor niches hosted by microbial mats

Received: 7 January 2019
Accepted: 12 August 2019
Published online: 20 September 2019

Weiming Ding[1,2], Lin Dong[1,2], Yuanlin Sun[1,2], Haoran Ma[1,2], Yihe Xu[1,2], Runyu Yang[1,2], Yongbo Peng[3], Chuanming Zhou[4] & Bing Shen[1,2]

The earliest unambiguous evidence for animals is represented by various trace fossils in the latest Ediacaran Period (550–541 Ma), suggesting that the earliest animals lived on or even penetrated into the seafloor. Yet, the O_2 fugacity at the sediment-water interface (SWI) for the earliest animal proliferation is poorly defined. The preferential colonization of seafloor as a first step in animal evolution is also unusual. In order to understand the environmental background, we employed a new proxy, carbonate associated ferrous iron (Fe_{carb}), to quantify the seafloor oxygenation. Fe_{carb} of the latest Ediacaran Shibantan limestone in South China, which yields abundant animal traces, ranges from 2.27 to 85.43 ppm, corresponding to the seafloor O_2 fugacity of 162 μmol/L to 297 μmol/L. These values are significantly higher than the oxygen saturation in seawater at the contemporary atmospheric pO_2 levels. The highly oxygenated seafloor might be attributed to O_2 production of the microbial mats. Despite the moderate atmospheric pO_2 level, microbial mats possibly provided highly oxygenated niches for the evolution of benthic metazoans. Our model suggests that the O_2 barrier could be locally overcome in the mat ground, questioning the long-held belief that atmospheric oxygenation was the key control of animal evolution.

The last 10 million years of the Ediacaran Period (550–541 Ma), at the eve of Cambrian Explosion, experienced dramatic and enigmatic changes in the biosphere[1,2]. The classic Ediacaran biota showed a sharp decline in diversity[3], and the earliest unambiguous bilaterian animals—represented by various types of trace fossils[4,5]—began to occupy ecological niches on the seafloor. For example, the first U-shaped trace fossil, *Arenicolites* from Western Mongolia, indicates that early animals had the ability to burrow vertically into sediments[6], and the oldest trackways from South China imply the presence of bilaterian animals with paired appendages[7].

Recent Uranium (U) isotope studies indicated there was extensive oceanic anoxia (>21% of the seafloor) during terminal Ediacaran, which was associated with the decline of Ediacaran biota[8]. There are also previous studies suggesting that, although atmospheric pO_2 level remained modest, varying between 10–40% Present Atmospheric Level (PAL)[9,10], the deep ocean remained predominantly anoxic[11], and the ocean oxidation was episodic throughout the Ediacaran and Cambrian[12,13]. The full oxygenation of the ocean-atmosphere system did not occur until the latter Pleozoic[9]. Although some geochemical evidences have been interpreted as increased oxygenation during the terminal Ediacaran[14–16], redox conditions adjacent to the sediment-water interface (SWI) is still poorly constrained.

The O_2 fugacity of the modern seafloor is highly heterogeneous (0 ~ >250 μmol/L)[17], suggesting that atmospheric oxygenation and seawater oxidation does not necessarily mean high seafloor O_2 fugacity. Existing geochemical proxies, such as Fe-S-C systematics[12,18,19], molybdenum isotopes[20], Ce anomalies[21], nitrogen isotopes[22] and abundance of redox-sensitive trace elements[23], reflect the degree of seawater oxidation, but make no direct inference about the seafloor redox. The earliest mobile animals, represented by the occurrence of Ediacaran and early Cambrian trace fossils, predominantly have benthic rather than pelagic lifestyle[24,25]. Yet, it remains unclear

[1]Key Laboratory of Orogenic Belts and Crustal Evolution, MOE, Beijing, 100871, China. [2]School of Earth and Space Science, Peking University, No. 5 Yiheyuan Road, Haidian District, Beijing, 100871, China. [3]Department of Geology and Geophysics, Louisiana State University, Baton Rouge, Louisiana, 70803, USA. [4]Key Laboratory of Economic Stratigraphy and Palaeogeography, Nanjing Institute of Geology and Palaeontology, Chinese Academy of Sciences, Nanjing, 210008, China. Correspondence and requests for materials should be addressed to L.D. (email: lin.dong@pku.edu.cn)

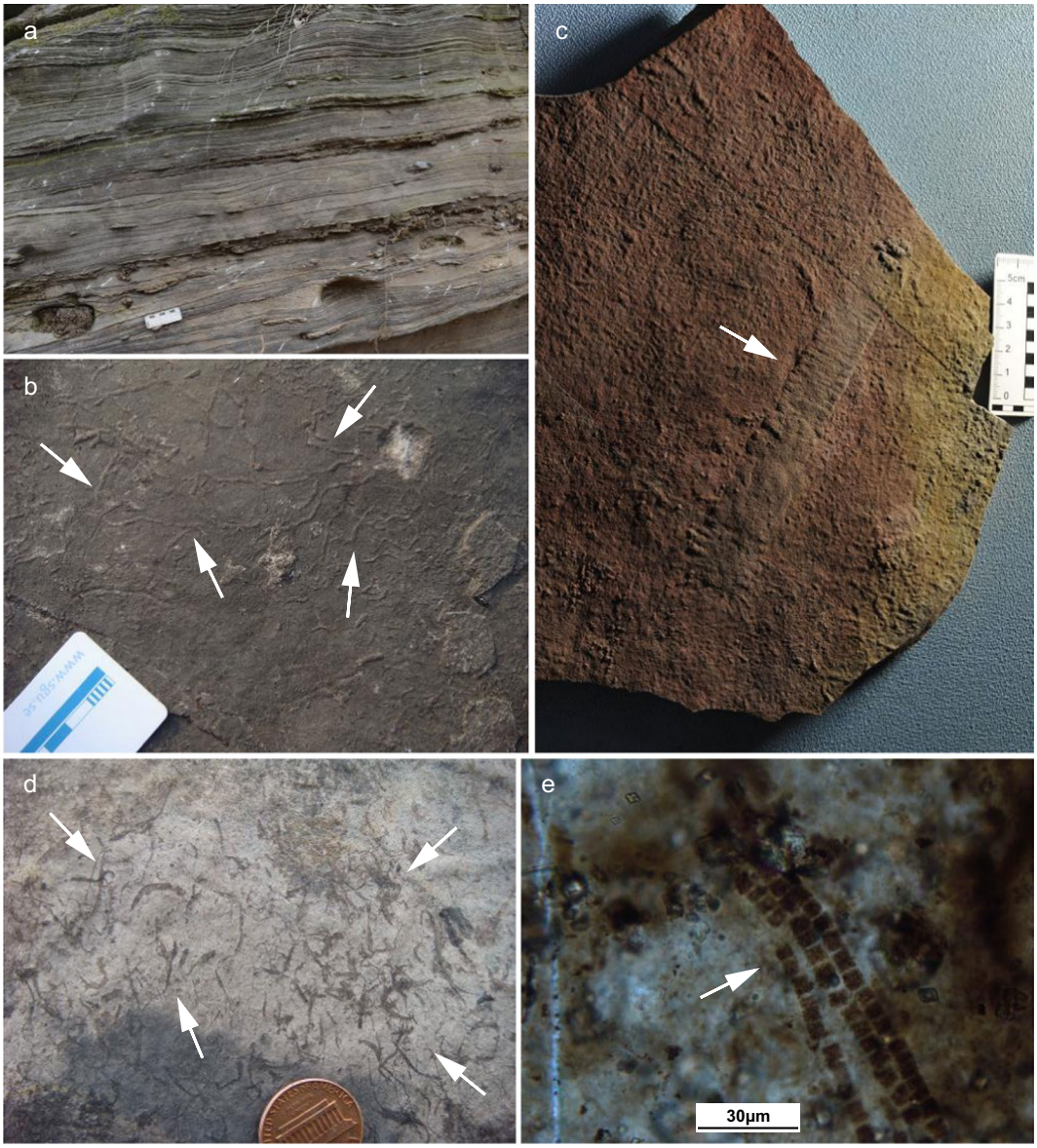

Figure 1. Lithology and fossils of the Shibantan Member, Dengying Formation. (**a**) Dark, laminated organic-rich limestone; (**b**) Abundant trace fossils (white arrows); (**c**) *Wutubus annularis*. White arrow points to apex; (**d**) *Vendotaenia* (white arrows); (**e**) Typical benthic cyanobacteria *Oscillatoria* from the chert nodules in the Denying limestone (white arrow).

what exactly were the oxygen conditions under which the animals, especially benthos that live on the SWI or even penetrate into the sediment, survived and radiated in the terminal Ediacaran ocean.

In order to understand the environmental conditions experienced by the earliest benthic animals, we propose a method of retrieving the seafloor O_2 fugacity from sections where the earliest animals evolved. The Ediacaran Dengying Formation (551–541 Ma), Yangtze Block, South China, contains abundant trace fossils together with both canonical and atypical Ediacaran fossils[4,26,27]. These fossils are particularly well known from in the bituminous limestone of the Shibantan Member (Fig. 1). In addition, the earliest biomineralized organism, *Cloudina*, has been discovered in the Baimatuo Member of the uppermost Dengying Formation[28–31]. As one of the few terminal Ediacaran fossiliferous carbonate successions in the world, the Dengying limestone may provide a unique window to view the environmental and ecological background of the latest Ediacaran evolution. In this study, we developed a new proxy, carbonate associated ferrous iron (Fe_{carb}), to constrain the seafloor O_2 fugacity during the emergence of the earliest benthic animals in the latest Ediacaran Dengying Formation in South China.

Fe_{carb} As A Proxy of Seafloor O_2 Fugacity

Ferrous Fe [Fe(II)] is thermodynamically unstable in oxic conditions, and would be oxidized to ferric Fe [Fe(III)], resulting in the precipitation of iron oxides or iron oxyhydroxides at neutral to alkaline pH conditions. The redox equilibrium between Fe^{2+} and O_2 could be expressed as:

$$4Fe^{2+} + O_2 + 10H_2O \rightarrow 4Fe(OH)_3 + 8H^+ \quad (1)$$

Thus, modern oxic seawater have extremely low dissolved Fe content (0~1.5 nmol·L^{-1})[32]. Ferric Fe can be reduced by iron reducing microbes (IRM) in suboxic-anoxic sediments by process collectively known as the dissimilatory iron reduction (DIR)[33]. The chemical reaction of DIR can be expressed as:

$$2Fe_2O_3 + CH_2O + 3H_2O \rightarrow 4Fe^{2+} + HCO_3^- + 7OH^- \quad (2)$$

DIR generates Fe^{2+}, increasing Fe^{2+} concentration in sediment porewater (0~500 μmol·L^{-1} in modern ocean)[34,35]. As such, high porewater Fe^{2+} content and low seawater Fe^{2+} content generate a Fe^{2+} concentration gradient, which results in the upward diffusion of dissolved Fe^{2+} and a benthic Fe^{2+} flux. The concentration gradient of Fe^{2+} (∇_{Fe}) can be expressed by the following simplified equation:

$$\nabla_{Fe} = \frac{([Fe]_{pw} - [Fe]_{sw})}{l_{Fe}} \quad (3)$$

where l_{Fe} is the depth of the upper boundary of DIR zone below SWI. $[Fe]_{pw}$ and $[Fe]_{sw}$ are Fe^{2+} concentration in porewater (within the DIR zone) and seawater, respectively. $[Fe]_{pw}$ is determined by the availability of ferric Fe oxides/oxyhydroxides and organic matter (Eq. 2). Considering the large difference in the order of magnitudes between $[Fe]_{pw}$ and $[Fe]_{sw}$, the concentration gradient is mainly controlled by $[Fe]_{pw}$ as follows:

$$\nabla_{Fe} = \frac{[Fe]_{pw}}{l_{Fe}} \quad (4)$$

The benthic flux of Fe^{2+} ($Flux_{Fe}$) can be expressed as:

$$Flux_{Fe} = \nabla_{Fe} \times D_{Fe} \quad (5)$$

where D_{Fe} is the diffusivity coefficient of Fe^{2+} in porewater. At equilibrium, Eq. 1 can be written as:

$$K = \frac{[H^+]^8}{[Fe^{2+}]^4 \times [O_2]} \quad (6)$$

where K is the equilibrium constant. The Fe^{2+} concentration shows an inversely exponential relationship with the O_2 content. Rearranging Eqs 4–6, we arrive at:

$$Flux_{Fe} = D_{Fe} \times \frac{[H^+]^2}{l_{Fe} \times (K \times [O_2])^{1/4}} \quad (7)$$

Thus, in theory, when pH and temperature remain unchanged, there is an inversely exponential relationship between benthic iron flux ($Flux_{Fe}$) and bottom water O_2 ($O_{2\text{-}BW}$) adjacent to the SWI, which can be expressed as an empirical equation:

$$Flux_{Fe} = a \times (O_{2-BW})^b \quad (8)$$

In the modern ocean, there exists a negative correlation between $O_{2\text{-}BW}$ and $Flux_{Fe}$[36–38] (Supplementary Fig. 6). Instead of using *in situ* fluxes, we collected the benthic flux data measured by non-invasive benthic chambers[39]. Strong benthic bioturbation related with water depth in the modern ocean can elevate the iron flux (Supplementary Fig. 6). In order to recede the influence of benthos, we choose the data collected from locations with water depth greater than 500 m. Thus, the best fitted power function can be expressed as follows (see supplementary text; Supplementary Fig. 7; the units of $Flux_{Fe}$ and $O_{2\text{-}BW}$ are mol·m^{-2}·Myr^{-1} and mol·L^{-1}):

$$Flux_{Fe} = 10^{-4.98\pm0.72} \times (O_{2-BW})^{-1.71\pm0.16} \quad (9)$$

We suggest that $Flux_{Fe}$ could be recorded by carbonate precipitating on the seafloor. Because Fe^{2+} and Ca^{2+} have similar ionic radii and charge, Fe^{2+} has the tendency to replace Ca^{2+} in carbonate minerals[40]. Fe_{carb} is determined by Fe^{2+} concentration in solution that is related to the redox condition (or oxygen fugacity) and the partitioning coefficient that is temperature, pH, Eh and mineralogy dependent[41]. Because $[Fe]_{pw}$ is at least 3 orders of magnitude larger than $[Fe]_{sw}$, benthic flux (with Fe^{2+} flux of 0.02~568 μmol·m^{-2}·d^{-1} in the modern ocean) would be the major Fe source for benthic carbonates. Equation for Fe_{carb} of seafloor carbonate precipitation can be expressed as (see supplementary text):

$$Fe_{carb} = \frac{K_{Fe} \times M_{Fe} \times 10^{-4.98} \times (O_{2-BW})^{-1.71}}{s \times \rho} \quad (10)$$

where K_{Fe} is the partitioning coefficient of the benthic Fe^{2+} flux into the carbonate lattice. M_{Fe} is the molecular weight of Fe (56 g/mol), s is the sedimentation rate, and ρ is the density of carbonates (2.71 g/cm^3).

Notably, although Fe_{carb} content is determined by the seafloor O_2 fugacity, which is controlled—although not uniquely—by the atmospheric pO_2 level, the quantitative reconstruction of atmospheric pO_2 level by using Fe_{carb} is not directly applicable. On one hand, Fe speciation in seawater is complex. In addition to free Fe^{2+}, the

dissolved ferrous Fe species also include various Fe-organic complexes, which accounts for the majority of the dissolved Fe in the modern ocean[32]. On the other hand, atmospheric pO_2 level is not the only control of bottom seawater redox. Instead, both organic matter influx and ocean circulation also play important roles[42]. If the water column above the SWI enriches organic matter or ocean circulation is stagnant, there can be decoupling between atmospheric pO_2 level and bottom water O_2 content. Therefore, Fe_{carb} can only constrain the redox conditions on the seafloor, and not in the atmosphere.

Furthermore, using Fe_{carb} to reconstruct seafloor O_2 fugacity can only be applied to carbonate that precipitated on the seafloor. Before the evolution of skeletonizing organisms, i.e. Ca-carbonate biomineralization in the latest Ediacaran[43,44], marine carbonate precipitation derive from biotically induced carbonate precipitation and direct abiotic precipitation from seawater or porewater[45]. The inorganic precipitation, identified by crystal fan and herringbone structures in carbonate, was common in Archean and decreased in abundance after the late Paleoproterozoic[46]. By contrast, biotically induced precipitation is driven by an elevation of carbonate saturation resulting from releasing of microbial metabolite into carbonate producing micro-environments[47,48]. The Shibantan limestone contains abundant organic-rich filaments, and is composed of crinkled microlaminae that have been interpreted as microbial mats[7,27,49] (Fig. 2). It is reasonable to argue that the Dengying carbonate precipitation was triggered by benthic microbes on the seafloor, warranting the application of Fe_{carb} to reconstruct seafloor O_2 fugacity. Furthermore, before the evolution of pelagic planktonic carbonate secreting organisms in Mesozoic, nearly all marine carbonate in the Paleozoic ocean was generated by benthic calcifiers, such as brachiopods, corals, and echinoderms[50]. Although carbonates precipitation from the water column cannot be completely ruled out, physical and biological abrasions of biogenic carbonate should be the major source of carbonate mud (i.e. micrite) in the Paleozoic ocean[51]. Therefore, Fe_{carb} of micrite from the Paleozoic carbonate can be used to reconstruct the seafloor O_2 fugacity as well. In this study, we use Fe_{carb} of the late Paleozoic (late Devonian and early Carboniferous) limestone (see supplementary text; Supplementary Fig. 3) as references. It is reasonable to speculate that the concentration of dissolved oxygen in the late Paleozoic shallow water was in equilibrium with the atmosphere, whose pO_2 levels were at least comparable to or even higher than that of the modern atmosphere[9].

It should be noted that there are limitations and assumptions when applying Fe_{carb} to reconstruct the seafloor O_2 fugacity. First, considering the short residence time of dissolved iron in seawater (on the order of 100~200 yr)[52], Fe_{carb} only reflects the local seafloor redox rather than the global state which can be estimated by uranium isotopes[53]. Second, Eq. 10 is based on the assumption of unlimited benthic Fe^{2+} flux. However, benthic Fe^{2+} flux would be finite when there are deficient supplies of reactive Fe or organic matter. In this case, low Fe_{carb} could also be generated at low seafloor O_2 fugacity with insufficient supplies of reactive Fe or organic matter. Thus, the interpretation of Fe_{carb} data should also consider siliciclastic and TOC contents in carbonate so as to guarantee sufficient Fe flux from sediment porewater. Third, we suggest that Fe_{carb} can only be applied to limestone rather than dolostone. Generally higher Fe_{carb} of dolostone may not only be the consequence of Fe-enriched dolomitization fluid, but also result from higher miscibility between Mg and Fe in carbonate lattice than between Ca and Fe[40]. Possibly multiple stages and fluid origins of dolomitization also interfere Fe_{carb} as a seafloor redox indicator. Thus, we recommend samples with low Mg/Ca (<0.05) should be selected. Finally, authigenic carbonate precipitation within DIR zone that has high Fe^{2+} content could also contribute to higher Fe_{carb}. Therefore, Fe_{carb} represents the minimum estimation of the seafloor $O_{2\text{-}BW}$.

Geological Setting and Sample Description

The Dengying Formation in the Yangtze Gorges area can be divided into, in ascending order, the Hamajing, Shibantan and Baimatuo members[30] (Supplementary Fig. 2). The Shibantan Member, sandwiched between the peritidal dolostone of the Hamajing and Baimatuo members, is composed of dark, laminated, organic-rich limestone. The Shibantan limestone contains a variety of fossils, including trace fossils, Ediacara fossils (e.g. *Wutubus annularis*), algal fossils (e.g. *Vendotaenia*), as well as benthic cyanobacteria (e.g. *Oscillatoria*) (Fig. 1). The absence of subaerial exposure structures as well as the occasional occurrences of hummocky cross bedding suggests the deposition in a deep subtidal environment, probably below the fair-weather wave base but above the storm-wave base (Fig. 2; see Supplementary Text).

Samples were collected from the Sixi and Huangniuyan sections in the Yangtze Gorges area, South China (Fig. 2a–d; Supplementary Fig. 1). The fine laminae are confined by organic-rich microbial filaments and are composed of alternating micritic and calcspar layers (Fig. 2e–h). The micritic layer normally has higher organic and siliciclastic contents, while the calcspar layer is composed of subhedral-anhedral calcite crystals of up to 100 μm in size. The calcspar crystals usually have fuzzy boundaries and contain abundant remaining micrites, suggesting the calcspar might derive from recrystallization of micrite in the early stage of diagenesis.

Results

The micrite and calcspar layers of the Shibantan limestone have comparable Fe_{carb}, ranging from 2.27 ppm to 157.34 ppm (mean = 47.49 ppm, n = 22) and from 2.31 ppm to 260.15 ppm (mean = 57.12 ppm, n = 32), respectively (Supplementary Fig. 4; Supplementary Table 1). The limestone samples with Mg/Ca molar ratio < 0.05 have Fe_{carb} varying between 2.27 ppm and 85.43 ppm (mean = 22.48 ppm, n = 24) (Fig. 3). As a comparison, Fe_{carb} of the late Paleozoic carbonates shows a wide range of variation (Fig. 3; Supplementary Table 2). In general, samples from shallow water carbonate platform environment, including the Panlong, Madao and Dazhai sections, have lower Fe_{carb}, ranging from 15.28 ppm to 166.26 ppm (mean = 63.44 ppm, n = 31), whereas the equivalent deep water samples from the Duli, Xiada and Daposhang sections have significantly higher Fe_{carb}, varying between 373.01 ppm and 2471.23 ppm (mean = 924.42 ppm, n = 83) (Fig. 3; Supplementary Table 2).

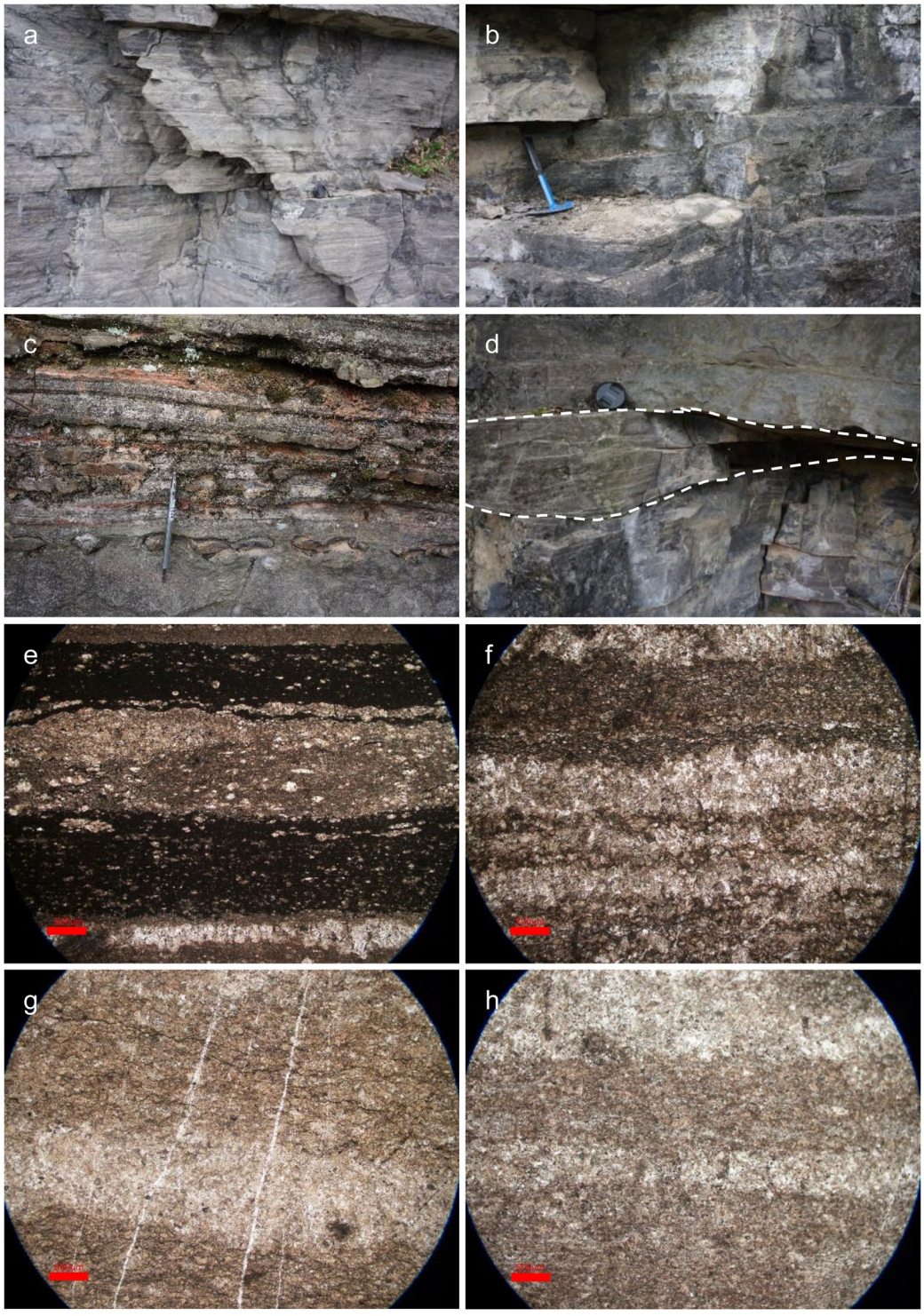

Figure 2. Field photographs and transmitted light photomicrographs. (**a**) Outcrop photograph showing the well-laminated limestone of the Shibantan Member, Dengying Formation. (**b**) Outcrop photograph showing dark-colored organic rich limestone. (**c**) Outcrop photograph showing the chert nodules in the limestone of the Shibantan Member, Dengying Formation. (**d**) Outcrop photograph showing hummocky cross beddings (dashed lines for orientation). (**e**,**f**) Photomicrograph showing organic rich micro-laminae of micrite and calcspar. Several calcspar-grains can be seen in the micritic layer. (**g**,**h**) photomicrograph showing alternating calcspar and micritic layers. The boundary between the laminae is fuzzy. Scale bars are 500 μm for pictures e–h.

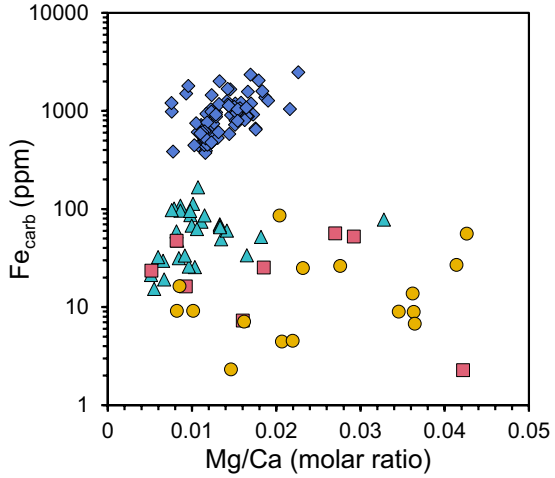

Figure 3. Fe_{carb} concentration of the Dengying Formation and carbonates in late Paleozoic including samples with Mg/Ca < 0.05. Crossplot showing Mg/Ca molar ratio(x-axis) vs. Fe_{carb} content(y-axis). Low Fe_{carb} content of micrite (red squares) and calcispar (yellow dots) layers of the Dengying Formation shows no significant difference, indicating that carbonates precipitated in Fe-depleted condition. Fe_{carb} content of shallow water carbonates in late Paleozoic (cyan triangles) is comparable to that of the Dengying Formation. Deep water carbonates in late Paleozoic (blue rhombuses) are characterized by high Fe_{carb}.

Discussion

The Shibantan limestone (Mg/Ca molar ratio < 0.05) samples have extremely low Fe_{carb} values both in micritic and calcspar layers, with little difference between these two types of layers, supporting the petrological observation that the calcspar mainly derives from recrystallization of micrite (Fig. 3). In addition, the Mn content in the Shibantan limestone is extremely low or even undetectable, suggesting little alteration by meteoric fluids[54] (Supplementary Table 1). Other diagenetic processes, which dominantly occur in anoxic conditions and cause more Fe^{2+} incorporation into the carbonate lattice, would most likely elevate Fe_{carb}. Therefore, low Fe_{carb} of the Dengying limestone may not result from diagenetic processes.

Low Fe_{carb} of the Dengying limestone cannot be attributed to oceanic euxinia as well (i.e. H_2S enriched but Fe^{2+} depleted), because abundant trace fossils and macroscopic Ediacara fossils strongly argue for a non-sulfidic environment[4,26,49]. Neither could the low Fe_{carb} be attributed to low $[Fe]_{pw}$ resulting from insufficient supply of organic matter and reactive Fe. Firstly, the Dengying limestone has high siliciclastic contents (average = 14.34%, n = 47; Supplementary Table 4), suggesting sufficient reactive Fe in sediments (Supplementary Fig. 9). Secondly, high organic carbon content (average = 2.47%, n = 47, Supplementary Table 4) in bituminous limestone warrants DIR in sediment porewater. In addition, low Fe_{carb} of the Shibantan limestone (mean = 22.48 ppm, n = 24) is close to, or even lower than that of the late Paleozoic shallow water carbonates (mean = 63.44 ppm, n = 31; Fig. 3). Considering the sedimentation rates of the Shibantan limestone (at least 24 m/Myr) and shallow marine carbonates in the Late Paleozoic sections (12.5 m/Myr for the Madao section, 6.4 m/Myr for Panlong section and 28.6 m/Myr for Dazhai section), the Ediacaran seafloor O_2 fugacity should be comparable to that of the well ventilated seafloor in Late Paleozoic (Eq. 10). Thus, low Fe_{carb} of the Shibantan limestone can only be explained by high seafloor O_2 fugacity.

To quantify the seafloor O_2 fugacity by Eq. 10, K_{Fe} should be determined in advance. However, K_{Fe} that specifically represents partition coefficient of benthic Fe^{2+} incorporation into calcite has not been directly determined for modern limestone, although the factors affecting Fe^{2+} incorporation into calcite in aqueous solution at equilibrium state have been investigated[55,56]. To constrain this unknown, we use Fe_{carb} data of late Devonian-early Carboniferous shallow marine carbonate samples (Madao, Panlong and Dazhai sections), to calculate the K_{Fe}. The calculated K_{Fe} value is then validated by the equivalent deep water carbonate samples (Duli, Xiada and Daposhang sections), which were collected from the beddings that contains abundant benthic animal fossils and thus were also inferred to represent oxic conditions (Fig. 3; see supplementary text; Supplementary Table 2). The result shows that the average K_{Fe} is 2.32 (1.86 for Madao section, 1.89 for Panlong section and 3.22 for Dazhai section). These calculated K_{Fe} values are within the range of values previously determined by experimental studies (1.5–2.3 at 10 °C and 2.8–7.7 at 50 °C)[55]. To reconstruct $O_{2\text{-}BW}$ during the deposition of carbonates by Eq. 10, we use $K_{Fe} = 2.32$ and s = 5, 10, 20, 40 m/Myr. $O_{2\text{-}BW}$ of 6.25 μmol/L is set as the upper bound of anoxic and euxinic conditions (i.e. microbial sulfate reduction occurs below this threshold)[17] and 68 μmol/L as the cutoff for the suboxic and oxic conditions[57,58]. The modeling result displays a negatively exponential relationship between Fe_{carb} and $O_{2\text{-}BW}$ (Fig. 4). Indeed, we cannot completely exclude carbonate precipitation from the water column, which will ultimately decrease Fe_{carb} due to low Fe^{2+} content in the seawater. Assuming that 80% of carbonate originally precipitates on the seafloor, and the other 20% precipitates from the water column, the colored area in Fig. 4 indicate the range of Fe_{carb} and $O_{2\text{-}BW}$ changes under different sedimentation rates.

Thus, the calculated $O_{2\text{-}BW}$ (average Fe_{carb} of 22.48 ppm for the Dengying limestone), i.e., the seafloor O_2 fugacity during terminal Ediacaran, ranges from 162 μmol/L to 297 μmol/L, when the sedimentation rate varies between 24 m/Myr and 67 m/Myr (see supplementary text; Supplementary Table 3). The upper bound (297 μmol/L) exceeds the saturated dissolved O_2 of 273 μmol/L in seawater at 1 PAL pO_2, while the lower bound

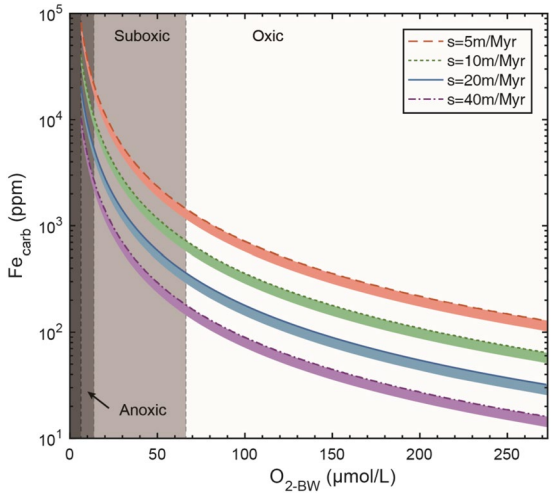

Figure 4. Modelling results according to the Eq. 10. Fe_{carb} trapped in the carbonate lattice (y-axis) varies as a function of the bottom water oxygen level ($O_{2\text{-}BW}$, x-axis). Contour lines indicate different sedimentation rate of carbonates. The lower limit of $O_{2\text{-}BW}$ was set at 6.25 μmol/L, the boundary of euxinia in the water column[21]. The upper limit of $O_{2\text{-}BW}$ was set at 273 μmol/L, the saturated O_2 level in the water column. Vertical dashed lines define the boundary of dissolved O_2 level for oxic (>68 μmol/L), suboxic (13.6 μmol/L~68 μmol/L) and anoxic (6.25 μmol/L~13.6 μmol/L) conditions[49,50]. The color areas suggest the possible relationship between Fe_{carb} and $O_{2\text{-}BW}$ if we assume that 20% of carbonate formed in the water column. See texts for more information.

(162 μmol/L) is equivalent to the dissolved O_2 content at 60% PAL pO_2. If we assume that measured Fe_{carb} of the Dengying Formation is 20% lower than original benthic carbonates because of seawater carbonate mixing, the minimum seafloor O_2 fugacity is still 143 μmol/L. Thus, even if the Ediacaran atmospheric pO_2 level reaches the maximum estimate of 40% PAL[9], the seafloor O_2 fugacity during the deposition of the Shibantan limestone was likely oversaturated with respect to the atmospheric pO_2 level.

High seafloor O_2 fugacity during the deposition of the Shibantan limestone seems contradictory with the modest atmospheric pO_2 levels and extensive seafloor anoxia in Ediacaran and Cambrian[8,59]. Local seafloor oxygenation must require a continuous O_2 supply to maintain oxic status under such predominately anoxic condition. Inspired by a modern analog, Los Roques lagoon in Venezuela[60] has low O_2 concentration in water column and is colonized by O_2-generating cyanobacteria mat in floor, but the O_2 concentration in the mat ground could be four times higher than that in the water column. Here, we suggest that the seafloor oxygenation might result from the development of microbial mats on the seafloor during the precipitation of Shibantan limestone (Figs 1a,e, 5 and 6). Microbial mats generate O_2 that is ready to be emitted into the water column, resulting in partial oxygenation of the adjacent bottom water. In addition, the downward diffusion of O_2 produced by microbial mats would lower the redox boundary of DIR zone, reducing the intensity of benthic flux of Fe^{2+} (Fig. 6). This model is consistent with the widespread microbial structures, e.g. warty textures[26], microbial laminae[4], and benthic cyanobacteria (Fig. 1e) in the Dengying limestone.

It has been proposed that microbial mats might have played a key role in the preservation of Ediacara fossils (the death mask hypothesis)[61], and the disappearance of Ediacara fossils at the Ediacaran-Cambrian boundary might be related to the disappearance of microbial mats after the evolution of metazoans[2]. Here, our new model proposes an alternative, but not mutually exclusive, interpretation that microbial mats might also provide a more locally oxygenated environment in the context of generally low atmospheric pO_2 level and widespread seafloor anoxia. Thus, microbial mats on shallow marine seafloor may generate an oxygenated oasis that might have stimulated the diversification of metazoans, even when the atmospheric pO_2 level was only 10–40% PAL, barely meeting the threshold for animal evolution[16]. Therefore, it is plausible that the earliest animals would refrain from floating in the ocean that is primarily anoxic and is characterized by dramatic redox oscillation, and prefer utilizing O_2 and food on and within the microbial mat. Such a hypothesis is also supported by the widespread late Ediacaran trace fossils associated with microbial sedimentary structures[4,5], some of which may indicate activities under microbial mats[49]. Our hypothesis could also support that the majority of the earliest animals were evidenced by trace fossils which record benthic instead of pelagic ethology. The lack of pelagic body fossil records may reflect the ecological constraint of the terminal Ediacaran communities driven by the ocean redox, not just a result of taphonomy or poor preservation.

Finally, the rise of atmospheric pO_2 level, which was thought to provide the upper constraint on the redox of the ocean, has been regarded as the *priori* for the animal evolution. However, our study suggests that local seafloor O_2 fugacity might significantly exceed the saturated O_2 content at a given atmospheric pO_2 level, and the local seafloor oxygenation might be attributed to the development of microbial mats. If this is the case, seafloor oxidation and atmospheric oxygenation might be decoupled. It is highly probable that seafloor might have long been locally oxidized when atmospheric pO_2 level was still low, because oxygenic microbial mats, e.g. stromatolites, are believed to cover the shallow marine seafloor since Archean time[62]. Therefore, we suggest that atmospheric or oceanic oxygenation may not be the crucial control on the emergence of animals; instead, life may have played the central role in the evolution of habitable planet.

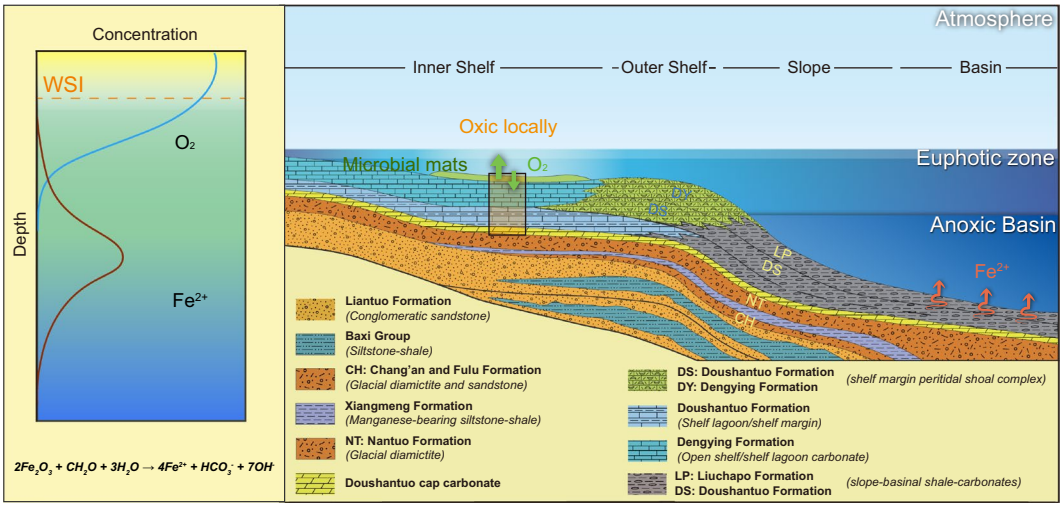

Figure 5. Schematic diagram illustrating the depositional environment of Dengying Formation (modified according to previous literatures[64,65]). The O_2 level in the atmosphere remained 10–40% PAL. The interface between atmosphere and water column could be slightly oxidized by the O_2 dissolution, whereas the majority part of the ocean still remained anoxic. Microbial mats, colonizing the seafloor where the Shibantan Member deposited, produced O_2 as benthic photosynthesis organism, which supersaturated the adjacent water column with O_2. In addition, the downward diffusion of O_2 would lower the redox boundary of iron reduction, reducing the benthic flux of Fe^{2+}.

Figure 6. Schematic diagram illustrating the biological oasis provided by microbial mats. O_2 bubbles produced by microbial mats diffused all around, making the ajancent water column partially oxidized. Oxygenation of uppermost sediments by downward diffusion of O_2 provided the niches for high ecological complexity of benthic communities. The Ediacara biota in the diagram all discovered in the Shibantan Member, Dengying Formation[4,26].

Methods

Elemental compositions measurement. Mirrored thin and thick sections were prepared for micro-mill sampling. Sample powders were micro-drilled from the thick section under the guide of thin section observation under optical microscopy. Based on the character of laminated limestone, two types of carbonate fabrics, micrite and calcispar, were sampled from the same specimen. About 50 mg of limestone powder was collected approximately in each sample and placed into a 15 ml centrifuge tube.

The sample preparation followed the sequential extraction procedure for carbonated associated Fe designed by Poulton and Canfield (2005)[63]. A buffer solution mixed by acetic acid (HAc) and ammonium acetate (NH_4Ac) was prepared, and the pH of 4.5 was adjusted accurately before use. For each sample, about 50 mg of sample powder was weighed and was dissolved in 10 ml buffer solution in a centrifuge tube. In order to ensure the solution has full contact with the sample, tubes were placed in a shaking table at 50 °C for 48 hours. After centrifugation, 0.5 ml supernatant was taken out and was mixed with 4.5 ml 2% nitric acid (HNO_3) in a new centrifuge tube. Finally, elemental compositions were measured with a Spectra Blue Sop Inductively Coupled Plasma Optical Emission Spectrometry (ICP-OES) at Peking University. All analyses were calibrated by a series of gravimetric standards with different concentrations (ranging from 0.1 ppm to 10 ppm) that were run before sample measurements.

TOC measurement. The limestone of the Dengying Formation was smashed into sample powder and about 100 mg of powder for each sample was weighed and was placed into a 50 ml centrifuge tube. To fully remove the inorganic carbon, 20 ml hydrochloric acid (HCl, 3N) was added to each centrifuge tube, which was then placed in an ultrasonic bath for 1 hour. The reaction was allowed for 12 hours. Then Milli-Q water (18.2 MΩ) was used to rinse the powders until pH reaches 4–5. After that, samples were dried overnight and loaded into capsules for TOC analysis at the Stable Isotope Research Facility (SIRF) at Louisiana State University, USA. Elemental analyzer (Micro Vario Cube, Isoprime Ltd., Cheadle, UK) flash-combust the samples in Tin capsule in a 950 °C furnace. Isoprime 100 (Isoprime 100, Cheadle, UK) gas source mass spectrometer can analyze the resulting CO_2 by continuous flow. The analyzed precision for TOC data is within 0.3%.

Data Availability

All data is available in the main text or the supplementary materials.

References

1. Xiao, S. & Laflamme, M. On the eve of animal radiation: phylogeny, ecology and evolution of the Ediacara biota. *Trends Ecol. Evol.* **24**, 31–40 (2009).
2. Laflamme, M., Darroch, S. A. F., Tweedt, S. M., Peterson, K. J. & Erwin, D. H. The end of the Ediacara biota: Extinction, biotic replacement, or Cheshire Cat? *Gondwana Res* **23**, 558–573 (2013).
3. Shen, B., Dong, L., Xiao, S. & Kowalewski, M. The Avalon explosion: evolution of Ediacara morphospace. *Science* **319**, 81–84 (2008).
4. Chen, Z. *et al*. Trace fossil evidence for Ediacaran bilaterian animals with complex behaviors. *Precambrian Res.* **224**, 690–701 (2013).
5. Macdonald, F. A., Pruss, S. B. & Strauss, J. V. Trace Fossils with Spreiten from the Late Ediacaran Nama Group, Namibia: Complex Feeding Patterns Five Million Years Before the Precambrian–Cambrian Boundary. *J. Paleontol.* **88**, 299–308 (2015).
6. Oji, T. *et al*. Penetrative trace fossils from the late Ediacaran of Mongolia: early onset of the agronomic revolution. *R. Soc. Open Sci.* **5**, 172250 (2018).
7. Chen, Z., Chen, X., Zhou, C., Yuan, X. & Xiao, S. Late Ediacaran trackways produced by bilaterian animals with paired appendages. *Sci Adv* **4** (2018).
8. Zhang, F. *et al*. Extensive marine anoxia during the terminal Ediacaran Period. *Sci Adv* **4**, eaan8983 (2018).
9. Sperling, E. A. *et al*. Statistical analysis of iron geochemical data suggests limited late Proterozoic oxygenation. *Nature* **523**, 451–454 (2015).
10. Kump, L. R. The rise of atmospheric oxygen. *Nature* **451**, 277–278 (2008).
11. Canfield, D. E. *et al*. Ferruginous conditions dominated later neoproterozoic deep-water chemistry. *Science* **321**, 949–952 (2008).
12. Sahoo, S. K. *et al*. Oceanic oxygenation events in the anoxic Ediacaran ocean. *Geobiology* (2016).
13. Kurzweil, F. *et al*. Coupled sulfur, iron and molybdenum isotope data from black shales of the Teplá-Barrandian unit argue against deep ocean oxygenation during the Ediacaran. *Geochim. Cosmochim. Acta* **171**, 121–142 (2015).
14. Shields-Zhou, G. A. & Och, L. M. The case for a Neoproterozoic oxygenation event: geochemical evidence and biological consequences. *GSA Today* **21**, 4–11 (2011).
15. Scott, C. *et al*. Tracing the stepwise oxygenation of the Proterozoic ocean. *Nature* **452**, 456–459 (2008).
16. Canfield, D. E., Poulton, S. W. & Narbonne, G. M. Late-Neoproterozoic deep-ocean oxygenation and the rise of animal life. *Science* **315**, 92–95 (2007).
17. Libes, S. *Introduction to marine biogeochemistry*. 2nd edn, (Academic Press, 2009).
18. Li, C. *et al*. A stratified redox model for the Ediacaran ocean. *Science* **328**, 80–83 (2010).
19. Wood, R. A. *et al*. Dynamic redox conditions control late Ediacaran metazoan ecosystems in the Nama Group, Namibia. *Precambrian Res.* **261**, 252–271 (2015).
20. Wen, H. *et al*. Molybdenum isotopic records across the Precambrian-Cambrian boundary. *Geology* **39**, 775–778 (2011).
21. Tostevin, R. *et al*. Low-oxygen waters limited habitable space for early animals. *Nat Commun* **7**, 12818 (2016).
22. Stueken, E. E., Kipp, M. A., Koehler, M. C. & Buick, R. The evolution of Earth's biogeochemical nitrogen cycle. *Earth Sci Rev* **160**, 220–239 (2016).
23. Robbins, L. J. *et al*. Trace elements at the intersection of marine biological and geochemical evolution. *Earth Sci Rev* **163**, 323–345 (2016).
24. Peterson, K. J., McPeek, M. A. & Evans, D. A. D. Tempo and mode of early animal evolution: inferences from rocks, Hox, and molecular clocks. *Paleobiology* **31**, 36–55 (2005).
25. Collins, A. G. & Valentine, J. W. Defining phyla: evolutionary pathways to metazoan body plans. *Evolution & Development* **3**, 432–442 (2001).
26. Chen, Z. *et al*. New Ediacara fossils preserved in marine limestone and their ecological implications. *Sci. Rep.* **4**, 4180 (2014).
27. Duda, J. P. *et al*. Geobiology of a palaeoecosystem with Ediacara-type fossils: The Shibantan Member (Dengying Formation, South China). *Precambrian Res.* **255**, 48–62 (2014).
28. Bengtson, S. & Zhao, Y. Predatorial borings in late Precambrian mineralized exoskeletons. *Science(Washington)* **257**, 367–369 (1992).
29. Hua, H., Chen, Z., Yuan, X. L., Zhang, L. Y. & Xiao, S. H. Skeletogenesis and asexual reproduction in the earliest biomineralizing animal Cloudina. *Geology* **33**, 277–280 (2005).

30. Zhao, Z. *et al*. *The Sinian System of Hubei*. Vol. 205 (China University of Geosciences Press, Wuhan, 1988).
31. Chen, M., Chen, Y. & Qian, Y. Some tubular fossils from Sinian–Lower Cambrian boundary sequences, Yangtze Gorge. *Bull. Tianjin Inst. Geol. Min. Res., Chinese Acad. Geol. Sci.* **3**, 117–124 (1981).
32. Tagliabue, A. *et al*. The integral role of iron in ocean biogeochemistry. *Nature* **543**, 51–59 (2017).
33. Lovley, D. R., Holmes, D. E. & Nevin, K. P. Dissimilatory Fe(III) and Mn(IV) reduction. *Adv. Microb. Physiol.* **49**, 219–286 (2004).
34. Morford, J. L., Martin, W. R. & Carney, C. M. Uranium diagenesis in sediments underlying bottom waters with high oxygen content. *Geochim. Cosmochim. Acta* **73**, 2920–2937 (2009).
35. Morford, J. L., Martin, W. R., Francois, R. & Carney, C. M. A model for uranium, rhenium, and molybdenum diagenesis in marine sediments based on results from coastal locations. *Geochim. Cosmochim. Acta* **73**, 2938–2960 (2009).
36. Severmann, S., McManus, J., Berelson, W. M. & Hammond, D. E. The continental shelf benthic iron flux and its isotope composition. *Geochim. Cosmochim. Acta* **74**, 3984–4004 (2010).
37. Elrod, V. A., Berelson, W. M., Coale, K. H. & Johnson, K. S. The flux of iron from continental shelf sediments: A missing source for global budgets. *Geophys. Res. Lett*. **31** (2004).
38. McManus, J., Berelson, W. M., Coale, K. H., Johnson, K. S. & Kilgore, T. E. Phosphorus regeneration in continental margin sediments. *Geochim. Cosmochim. Acta* **61**, 2891–2907 (1997).
39. Dale, A. W. *et al*. A revised global estimate of dissolved iron fluxes from marine sediments. *Glob Biogeochem Cycles* **29**, 691–707 (2015).
40. Clarkson, M., Poulton, S., Guilbaud, R. & Wood, R. Assessing the utility of Fe/Al and Fe-speciation to record water column redox conditions in carbonate-rich sediments. *Chem. Geol.* **382**, 111–122 (2014).
41. Barnaby, R. J. & Rimstidt, J. D. Redox Conditions of Calcite Cementation Interpreted from Mn-Contents and Fe-Contents of Authigenic Calcites. *GSAMB* **101**, 795–804 (1989).
42. Lenton, T. M., Boyle, R. A., Poulton, S. W., Shields-Zhou, G. A. & Butterfield, N. J. Co-evolution of eukaryotes and ocean oxygenation in the Neoproterozoic era. *Nat Geosci* **7**, 257–265 (2014).
43. Conway Morris, S., Mattes, B. W. & Chen, M. The early skeletal organism *Cloudina*: New occurrences from Oman and possibly China. *American Journal of Science* **290-A**, 245–260 (1990).
44. Grotzinger, J. P., Watters, W. A. & Knoll, A. H. Calcified metazoans in thrombolite-stromatolite reefs of the terminal Proterozoic Nama Group, Namibia. *Paleobiology* **26**, 334–359 (2000).
45. Bartley, J. K. & Kah, L. C. Marine carbon reservoir, C_{org}-C_{carb} coupling, and the evolution of the Proterozoic carbon cycle. *Geology* **32**, 129–132 (2004).
46. Sumner, D. Y. & Grotzinger, J. P. Herringbone calcite: petrology and environmental significance. *Journal of Sedimentary Research (Section A: Sedimentary Petrology and Processes)* **66**(3), 419–429 (1996).
47. Bergmann, K. D., Grotzinger, J. P. & Fischer, W. W. Biological influences on seafloor carbonate precipitation. *Palaios* **28**, 99–115 (2013).
48. Riding, R. Microbial carbonates: the geological record of calcified bacterial-algal mats and biofilms. *Sedimentology* **47**, 179–214 (2000).
49. Meyer, M. *et al*. Interactions between Ediacaran animals and microbial mats: Insights from Lamonte trevallis, a new trace fossil from the Dengying Formation of South China. *Palaeogeogr. Palaeoclimatol. Palaeoecol.* **396**, 62–74 (2014).
50. Tucker, M. E. & Wright, V. P. *Carbonate Sedimentology*. (1990).
51. Ridgwell, A. & Zeebe, R. The role of the global carbonate cycle in the regulation and evolution of the Earth system. *Earth Planet. Sci. Lett.* **234**, 299–315 (2005).
52. Boyd, P. W. & Ellwood, M. J. The biogeochemical cycle of iron in the ocean. *Nat Geosci* **3**, 675–682 (2010).
53. Andersen, M. B. *et al*. Closing in on the marine U-238/U-235 budget. *Chem Geol* **420**, 11–22 (2016).
54. Kaufman, A. J. & Knoll, A. H. Neoproterozoic variations in the C-isotopic composition of seawater: stratigraphic and biogeochemical implications. *Precambrian Res.* **73**, 27–49 (1995).
55. Dromgoole, E. L. & Walter, L. M. Iron and manganese incorporation into calcite: Effects of growth kinetics, temperature and solution chemistry ☆. *Chem Geol* **81**, 311–336 (1990).
56. Di Lorenzo, F., Burgos-Cara, A., Ruiz-Agudo, E., Putnis, C. V. & Prieto, M. Effect of ferrous iron on the nucleation and growth of CaCO3 in slightly basic aqueous solutions. *CrystEngComm* **19**, 447–460 (2017).
57. Sperling, E. A. *et al*. Oxygen, ecology, and the Cambrian radiation of animals. *Proc Natl Acad Sci USA* **110**, 13446–13451 (2013).
58. Kaiho, K. Benthic Foraminiferal Dissolved-Oxygen Index and Dissolved-Oxygen Levels in the Modern Ocean. *Geology* **22**, 719–722 (1994).
59. Wang, D. *et al*. Coupling of ocean redox and animal evolution during the Ediacaran-Cambrian transition. *Nat Commun* **9**, 2575 (2018).
60. Gingras, M. *et al*. Possible evolution of mobile animals in association with microbial mats. *Nat Geosci* **4**, 372–375 (2011).
61. Gehling, J. G. Microbial mats in terminal Proterozoic siliciclastics: Ediacaran death masks. *Palaios* **14**, 40–57 (1999).
62. Allwood, A. C. *et al*. Controls on development and diversity of Early Archean stromatolites. *Proc Natl Acad Sci USA* **106**, 9548–9555 (2009).
63. Poulton, S. W. & Canfield, D. E. Development of a sequential extraction procedure for iron: implications for iron partitioning in continentally derived particulates. *Chem Geol* **214**, 209–221 (2005).
64. Jiang, G., Shi, X., Zhang, S., Wang, Y. & Xiao, S. Stratigraphy and paleogeography of the Ediacaran Doushantuo Formation (ca. 635–551Ma) in South China. *Gondwana Res.* **19**, 831–849 (2011).
65. Lang, X. G. *et al*. Ocean oxidation during the deposition of basal Ediacaran Doushantuo cap carbonates in the Yangtze Platform, South China. *Precambrian Res.* **281**, 253–268 (2016).

Acknowledgements

We acknowledge Ting Nie and Jieqiong Chang for preparing the Paleozoic samples. We thank two reviewers whose comments/suggestions greatly helped improve and clarify this manuscript. Grants and contribution number: We acknowledge Natural Science Foundation of China (41672334 and 41402025).

Author Contributions

L. Dong conceived the study, W. Ding and L. Dong interpreted the data and drafted the work, W. Ding and H. Ma did the experiment, W. Ding, Y. Sun, H. Ma, R. Yang and Y. Xu collected samples, B. Shen, Y. Peng, and C. Zhou revised the manuscript.

Additional Information

Supplementary information accompanies this paper at https://doi.org/10.1038/s41598-019-49993-2.

Competing Interests: The authors declare no competing interests.

Publisher's note Springer Nature remains neutral with regard to jurisdictional claims in published maps and institutional affiliations.